Transcriptional profiling of Vero E6 cells over-expressing SARS-CoV S2 subunit: Insights on viral regulation of apoptosis and proliferation

Yin-Shan Yeung, Chi-Wai Yip, Chung-Chau Hon, Ken Y.C. Chow, Iris C.M. Ma,
Fanya Zeng, Frederick C.C. Leung *

Department of Zoology, Kadoorie Biological Science Building, The University of Hong Kong, Hong Kong

Abstract

We have previously demonstrated that over-expression of spike protein (S) of severe acute respiratory syndrome coronavirus (SARS-CoV) or its C-terminal subunit (S2) is sufficient to induce apoptosis *in vitro*. To further investigate the possible roles of S2 in SARS-CoV-induced apoptosis and pathogenesis of SARS, we characterized the host expression profiles induced upon S2 over-expression in Vero E6 cells by oligonucleotide microarray analysis. Possible activation of mitochondrial apoptotic pathway in S2 expressing cells was suggested, as evidenced by the up-regulation of cytochrome *c* and down-regulation of the Bcl-2 family anti-apoptotic members. Inhibition of Bcl-2-related anti-apoptotic pathway was further supported by the diminution of S2-induced apoptosis in Vero E6 cells over-expressing Bcl-xL. In addition, modulation of CCN E2 and CDKN 1A implied the possible control of cell cycle arrest at G1/S phase. This study is expected to extend our understanding on the pathogenesis of SARS at a molecular level.
© 2007 Elsevier Inc. All rights reserved.

Keywords: Severe acute respiratory syndrome coronavirus; Spike protein; Apoptosis; Proliferation; Microarray

Introduction

Severe acute respiratory syndrome (SARS) is a highly contagious disease caused by a member of the Coronaviridae family named SARS Coronavirus (SARS-CoV) (Drosten et al., 2003; Ksiazek et al., 2003; Peiris, 2003). The disease was first documented during late 2002 and the outbreak was effectively controlled by mid-2003 through rigorous quarantine measures (Zhong et al., 2003). However, the ability of the virus in infecting multiple cell types (Hattermann et al., 2005; Kaye, 2006) and animals (Martina et al., 2003) implied the risk of viral circulation in animal reservoirs and hence the re-emergence of the virus in human population. Understanding the molecular mechanisms of viral pathogenesis may provide important

information for rational design of antiviral drugs, which may be important to combat against another possible SARS epidemic. The viral–host factors contributing to the pathogenesis of SARS-CoV are incompletely understood. In addition to respiratory tract illness, lymphoid depletion in spleen and lymph nodes is a common clinical manifestation in fatal cases of SARS (Wong et al., 2003). Cytokine overdrive and apoptosis induced by the virus were suggested to contribute to such lymphoid depletion (Wong et al., 2003). These observations, together with the fact that SARS-CoV is capable to induce apoptosis in the viral susceptible Vero E6 cell line (Yan et al., 2004), highlighted the important role of apoptosis in the pathogenesis of SARS.

The SARS-CoV spike protein (S) is a class I fusion protein. Cellular entry of the virus was demonstrated to be mediated by S through the receptor binding domain located in the N-terminal subunit (S1) (Dimitrov, 2004; Hofmann and Pohlmann, 2004) and the fusion peptide in the C-terminal subunit (S2) (Dimitrov, 2004; Hofmann and Pohlmann, 2004). Recent studies also suggested the presence of neutralizing domains in S2 (Duan et al., 2005; Keng et al., 2005; Zeng et al., 2006; Zhang et al.,

* Corresponding author. Fax: +852 28574672.
E-mail addresses: ysyeung@graduate.hku.hk (Y.-S. Yeung),
h0024004@hkusua.hku.hk (C.-W. Yip), h9826299@hkusua.hku.hk
(C.-C. Hon), chow@pasteur.fr (K.Y.C. Chow), h0105962@hkusua.hku.hk
(I.C.M. Ma), fzeng@hkucc.hku.hk (F. Zeng), fcleung@hkucc.hku.hk
(F.C.C. Leung).

2004). We have previously demonstrated that the SARS-CoV S and S2, but not S1 nor other structural proteins, including envelope (E), membrane (M) and nucleocapsid (N), can induce apoptosis in Vero E6 cells (Chow et al., 2005). Other recent studies showed that the E (Yang et al., 2005), M (Lai et al., 2006; Zhao et al., 2006), N (Surjit et al., 2004; Zhao et al.,

2006), ORF 3a (Law et al., 2005), 3b (Yuan et al., 2005) and 7a (Tan et al., 2004) could trigger apoptosis in different cell lines or under specific culture conditions. As S is abundantly expressed during the virus replication cycle, and that the silencing of S expression exhibits an inhibition of cytopathic effect induced by SARS-CoV infection (He et al., 2006), we sought to elucidate
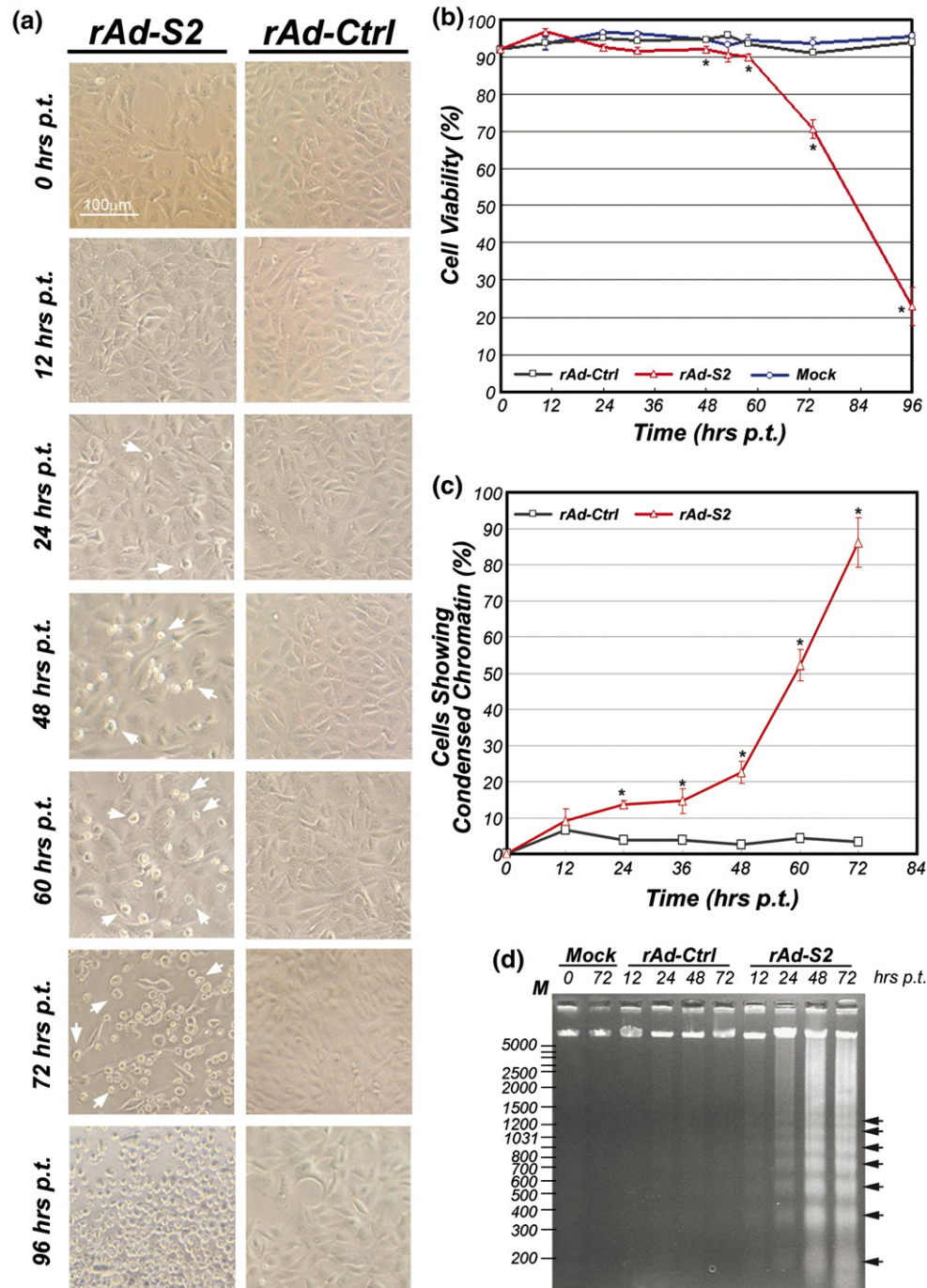

Fig. 1. Time course study of S2-induced apoptosis in Vero E6 cells. (a) Morphology of Vero E6 cells under light microscope (40×) after rAd-Ctrl or rAd-S2 transductions from 0 to 96 h p.t. in 12- to 24-h intervals. Representative figures of three independent experiments are shown. (b) Cell viability along the time course is estimated quantitatively with Trypan blue exclusion assay. (c) The percentage of rAd-Ctrl or rAd-S2-transduced cells showing chromatin condensation was counted under fluorescence microscope after Hoechst 33342 staining. For both panels b and c, average of three independent experiments is shown with standard error of the mean (SEM). (d) Agarose gel electrophoresis showing the characteristic DNA laddering pattern resulting from internucleosomal DNA cleavage in rAd-S2-transduced cells in four selected time points. Three micrograms of low molecular weight DNA was loaded into each well. The ladders with 200 bp increments are indicated with arrowheads. The result is the representative of three independent experiments. $*p < 0.01$ when compared with cells transduced by rAd-Ctrl under the same condition.

the molecular mechanisms of apoptosis mediated by S2 in Vero E6 cells.

In depicting the biochemistry of SARS-CoV infections, several microarray studies identified the differential expression of genes related to apoptosis, cell cycle and stress response in Vero (Leong et al., 2005), PBMC (Reghunathan et al., 2005; Yu et al., 2005) and Huh-7 cells (Tang et al., 2005). Other in vitro studies indicated that infection of SARS-CoV involves the phosphorylation of p38 MAPK (Mizutani et al., 2004b), down-regulation of Bcl-2 (Bordi et al., 2006; Ren et al., 2005), up-regulation of Bax and activation of caspase 3 (Ren et al., 2005). However, few efforts were put in trying to identify the role of individual proteins of SARS-CoV in these biochemical pathways. In this regard, using an adenoviral system for gene delivery, we studied the changes of expression profiles in serially sampled Vero E6 cells over-expressing S2 through microarray technology. Based on our results, we proposed the alternations of several physiological pathways that may be involved in S2-induced apoptosis, including the activation of intrinsic apoptotic pathway, inhibition of NFκB-downstream members and MAPK cascade members. Moreover, a number of genes critically involved in cell cycle control were also found to be differentially regulated.

Results and discussion

Apoptosis induced by SARS-CoV S2 over-expression

To determine the appropriate time points for microarray analysis, we first characterized the time-dependent induction of apoptosis by S2 over-expression mediated by recombinant adenoviruses (rAd). Starting from 24 h (h) post-transductions (p.t.), cytopathic effects, including abnormal cell morphology and shrinkage, were already observed in rAd-S2 but not rAd-Ctrl-transduced Vero E6 cells (Fig. 1a). Results of cell viability assay and chromatin condensation assay agreed well with the

above observations (Figs. 1b and c). Cell viability of rAd-S2-transduced cells dropped to the minimum at 96 h p.t. (Fig. 1b), and the percentage of rAd-S2-transduced cells undergoing apoptosis, as shown by chromatin condensation assay (Fig. 1c) and internucleosomal DNA cleavage analysis (Fig. 1d), increased rapidly and was peaked at 72 h p.t., which is the last time-point of the assays. According to these apoptotic signatures, which agree well with previous reports (Chow et al., 2005; Jamshidi-Parsian et al., 2005), four time points at 12, 24, 48 and 72 h p.t., were chosen for the microarray analysis.

The global gene expression profile in Vero E6 cells over-expressing SARS-CoV S2

A total of 1702 probe sets (3.2% of total probe sets) in the array have exhibited a significant up- or down-regulation (at least two-fold changes) in at least one of the time points upon S2 over-expression. Only 33 of these differentially hybridized probe sets showed both up- and down-regulation across the four time points, while the rest of them showed either only up (403 probe sets)- or down-regulated expression (1266 probe sets) during the course of the experiment. Gene ontology study classified 829 of the 1702 differential hybridized probe sets into 9 groups with known functions (Fig. 2) according to a defined classification (Tang et al., 2005). The relatively large number of unclassified probe sets may be due to the less characterized rhesus macaque genome, with unclassified probe sets and hypothetical proteins contributed to 33.6% and 7.1% of total probe sets respectively. Among the differentially hybridized probe sets with known function, 68 and 82 probe sets (representing 49 and 68 different genes, respectively), are related to apoptosis and cell cycle/proliferation respectively. The above data are summarized in Table 1. Changes of genes expression related to other cellular pathways in S2 expressing cells can be found in our Web page (http://evolution.hku.hk/publications/SARS_microarray.htm).
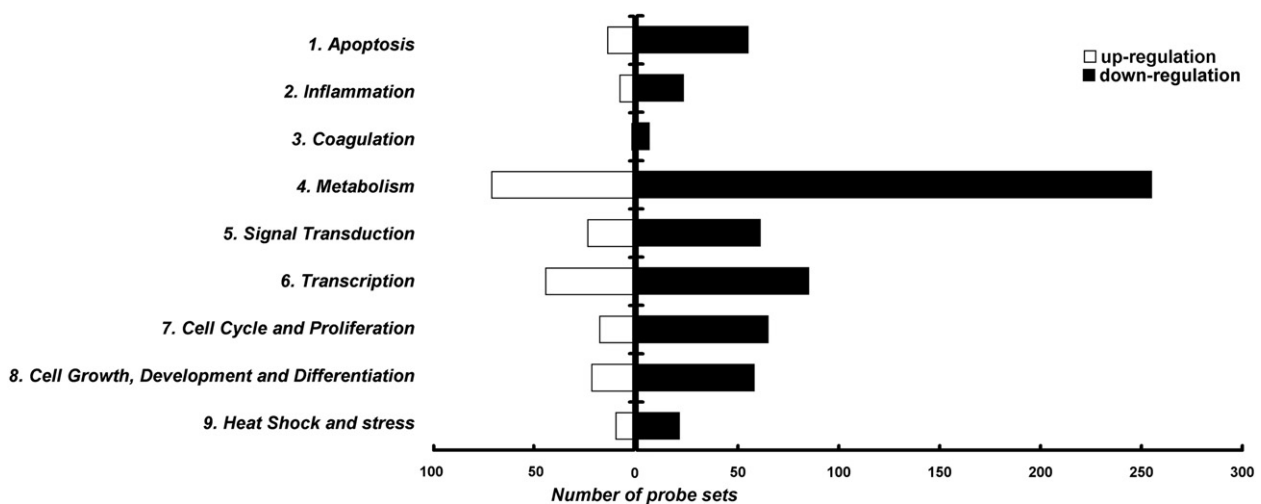
Fig. 2. Functional classification of differentially expressed probe sets. Probe sets that were differentially expressed by more than two-folds were classified into 11 groups manually, with 9 groups of known functions and two groups representing hypothetical/miscellaneous proteins and unknown proteins. The number of probe sets with known functions showing up- and down-regulations is shown with empty and filled bars respectively. The first group represents the probe sets related to apoptosis while probe sets regulating cell cycle and proliferation are grouped into group 7.

Table 1
Signal log ratios (log$_2$ scale) on the fold change of gene expression in S2-expressing Vero E6 cells (only genes highly related to apoptosis and cell cycle and proliferation are shown)

Categories and subcategories	Probe set ID	Gene symbol	Description	Log 2 ratio (sample/control)[a] (h p.i.)			
				12	24	48	72
Apoptosis							
Anti-apoptosis							
	MmugDNA.28580.1.S1_at	ANXA4	Annexin A4	−0.39	−0.28	−0.45	−1.01
	MmugDNA.34272.1.S1_s_at	API5	Apoptosis inhibitor 5	−1.44	−0.29	−0.36	−1.08
	MmugDNA.29603.1.S1_at	BCL2	B-cell CLL/lymphoma 2	0.40	−0.49	−1.24	−1.78
	MmugDNA.12133.1.S1_at	BCLXL	BCL2-like 1 (BCL2L1)	−1.56	−0.23	−0.77	−1.92
	MmugDNA.1928.1.S1_at	CTNNA1	Catenin (cadherin-associated protein), alpha 1, 102 kDa	−0.50	−0.08	−0.62	−1.22
	MmugDNA.39222.1.S1_at	CFL1	Cofilin 1 (non-muscle)	−1.11	−0.12	−0.53	−1.44
	MmugDNA.35450.1.S1_at	CSTB	Cystatin B (stefin B)	−1.03	−0.97	−0.85	0.01
	MmugDNA.21273.1.S1_at	HSPA5	Heat shock 70 kDa protein 5 (glucose-regulated protein, 78 kDa)	0.15	0.39	**1.88**	**2.15**
	MmugDNA.725.1.S1_at	HIPK3	Homeodomain interacting protein kinase 3	−2.13	−0.17	−0.17	−1.82
	MmugDNA.29385.1.S1_at	MIRN21	MicroRNA 21	−0.65	−0.22	−0.79	−1.12
	MmugDNA.38922.1.S1_at	MCL1	Myeloid cell leukemia sequence 1 (BCL2-related)	−0.95	−0.07	−0.48	−1.09
	MmugDNA.11909.1.S1_s_at	ARHGDIA	Rho GDP dissociation inhibitor (GDI) alpha	−1.35	−0.17	−1.17	−1.01
	MmugDNA.34988.1.S1_at	TXNDC	Thioredoxin domain containing	−1.40	0.02	−0.05	−1.11
	MmugDNA.40138.1.S1_at	TNFAIP3	Tumor necrosis factor, alpha-induced protein 3	0.57	0.45	0.72	**1.19**
	MmugDNA.32694.1.S1_at	TNFAIP8	Tumor necrosis factor, alpha-induced protein 8	−0.18	−0.69	−0.95	−1.46
	MmugDNA.30167.1.S1_at	TRA1	Tumor rejection antigen (gp96) 1	−0.24	0.42	**1.41**	0.93
	MmugDNA.6621.1.S1_at	TRA1	Tumor rejection antigen (gp96) 1	0.16	0.42	**1.41**	**1.14**
	MmugDNA.3345.1.S1_at	VEGF	Vascular endothelial growth factor	−0.94	−0.48	−0.05	−1.05
Pro-apoptosis							
	MmugDNA.6382.1.S1_at	BIRC3	Baculoviral IAP repeat-containing 3	−0.33	−0.37	−0.40	−1.05
	MmugDNA.30317.1.S1_at	BIRC4	Baculoviral IAP repeat-containing 4	**1.47**	0.28	0.53	**1.22**
	MmugDNA.2328.1.S1_at	BAG2	BCL2-associated athanogene 2	**1.12**	0.10	−0.12	0.65
	MmugDNA.4144.1.S1_s_at	BCL2L11	BCL2-like 11 (apoptosis facilitator)	−1.61	−0.49	−0.40	−0.85
	MmugDNA.23713.1.S1_at	BOMB	BH3-only member B protein	−0.99	−0.28	−0.57	−1.23
	MmugDNA.41236.1.S1_at	CASP2	Caspase 2, apoptosis-related cysteine peptidase (neural precursor cell expressed, developmentally down-regulated 2)	−0.72	0.35	−0.21	−1.40
	MmugDNA.13586.1.S1_at	CASP8	Caspase 8, apoptosis-related cysteine peptidase	−1.49	−0.45	−0.62	−1.38
	MmugDNA.15712.1.S1_x_at	CTSB	Cathepsin B	0.13	0.02	−0.07	**1.08**
	MmugDNA.19990.1.S1_s_at	CD99	CD99 antigen	−1.08	−0.24	−0.25	−1.28
	MmugDNA.15069.1.S1_at	CYCS	Cytochrome *c*, somatic	**1.50**	0.58	0.40	**1.63**
	MmugDNA.39077.1.S1_at	DAPK3	Death-associated protein kinase 3	−1.19	−0.68	−0.47	−0.37
	MmugDNA.29093.1.S1_at	DOC1	Down-regulated in ovarian cancer 1	−0.13	−0.31	−0.79	−1.53
	MmugDNA.24700.1.S1_at	ESRRBL1	Estrogen-related receptor beta like 1	−1.25	−0.32	−0.67	−1.51
	MmugDNA.7450.1.S1_at	FAF1	Fas (TNFRSF6) associated factor 1	−0.40	−0.60	−0.48	−1.08
	MmugDNA.34508.1.S1_at	HIP1	Huntingtin interacting protein 1	**1.10**	−0.02	0.11	0.47
	MmugDNA.38424.1.S1_at	IHPK2	Inositol hexaphosphate kinase 2	−0.23	−0.50	−0.60	−1.18
	MmugDNA.22620.1.S1_at	LGALS7	Lectin, galactoside-binding, soluble, 7 (galectin 7)	−0.10	−0.19	−0.53	−1.20
	MmugDNA.21644.1.S1_at	MAPK1	Mitogen-activated protein kinase 1	−1.41	−0.32	−0.27	−1.42
	MmugDNA.834.1.S1_at	RPL4	Mitogen-activated protein kinase kinase kinase 13	−1.75	−0.46	−0.41	−1.44
	MmugDNA.19461.1.S1_at	WIG1	p53 target zinc finger protein	−1.76	−0.73	−0.70	−1.94
	MmugDNA.22348.1.S1_at	PSEN1	Presenilin 1 (Alzheimer disease 3)	−1.00	−0.33	0.12	−0.61
	MmugDNA.5589.1.S1_at	PURB	Purine-rich element binding protein B	−0.90	−0.94	−1.14	−1.09
	MmugDNA.21841.1.S1_s_at	RHOB	Ras homolog gene family, member B	−1.44	−0.63	−0.86	−1.23
	MmugDNA.25692.1.S1_at	STK3	Serine/threonine kinase 3 (STE20 homolog, yeast)	−0.90	−0.15	−0.35	−1.02
	MmugDNA.39549.1.S1_at	STK4	Serine/threonine kinase 4	−1.89	−0.40	−0.61	−1.29
	MmugDNA.7204.1.S1_at	SGK	Serum/glucocorticoid regulated kinase	0.20	0.38	0.88	**1.38**
	MmugDNA.40778.1.S1_at	SH3MD2	SH3 multiple domains 2	**1.00**	−0.01	0.12	0.16
	MmugDNA.37821.1.S1_at	TNFRSF19	Tumor necrosis factor receptor superfamily, member 19	−1.47	−0.97	−0.84	−2.01
	MmugDNA.39342.1.S1_s_at	TNFRSF21	Tumor necrosis factor receptor superfamily, member 21	−0.42	−0.26	−0.74	−1.17
	MmugDNA.34645.1.S1_s_at	ZFP36L1	Zinc finger protein 36, C3H type-like 1	−0.16	−0.41	−0.73	−1.05
DNA repair							
	MmugDNA.12810.1.S1_at	BRCA2	Breast cancer 2, early onset	−1.18	−0.52	0.26	−0.17
Cell cycle and proliferation							
	MmugDNA.880.1.S1_at	ADAMTS1	ADAM metallopeptidase with thrombospondin type 1 motif, 1	−0.04	−0.32	−1.36	−2.22

(continued on next page)

Table 1 (*continued*)

Categories and subcategories	Probe set ID	Gene symbol	Description	Log 2 ratio (sample/control)[a] (h p.i.)			
				12	24	48	72
Apoptosis							
	MmugDNA.18873.1.S1_at	APBB2	Amyloid beta (A4) precursor protein-binding, family B, member 2 (Fe65-like)	−0.85	−0.33	−0.54	−1.02
	MmugDNA.40593.1.S1_at	ANAPC5	Anaphase promoting complex subunit 5	−1.21	−0.18	−0.36	−1.03
	MmugDNA.25197.1.S1_at	ASPM	Asp (abnormal spindle)-like, microcephaly associated (*Drosophila*)	**1.14**	−0.23	−0.16	0.64
	MmugDNA.27494.1.S1_at	BTBD7	BTB (POZ) domain containing 7	−1.60	−0.32	−0.77	−1.95
	MmugDNA.40767.1.S1_at	BUB3	BUB3 budding uninhibited by benzimidazoles 3 homolog (yeast)	−1.02	−0.24	−0.41	−0.94
	MmugDNA.24430.1.S1_at	CDC25A	Cell division cycle 25A	0.46	0.83	**1.08**	**1.55**
	MmugDNA.8073.1.S1_at	CDC25C	Cell division cycle 25C	−1.00	−0.86	−0.46	−1.49
	MmugDNA.7114.1.S1_at	CDCA2	Cell division cycle associated 2	−0.54	−0.83	−1.44	−0.18
	MmugDNA.15060.1.S1_at	CEP1	Centrosomal protein 1	**1.01**	−0.02	−0.21	0.54
	MmugDNA.27098.1.S1_at	CCND1	Cyclin D1	**1.04**	0.56	0.20	0.76
	MmugDNA.8564.1.S1_at	CCNE2	Cyclin E2	−1.34	0.22	0.25	−0.82
	MmugDNA.38294.1.S1_at	CCNG2	Cyclin G2	−1.56	−0.63	0.01	−2.04
	MmugDNA.14485.1.S1_at	CDK6	Cyclin-dependent kinase 6	−1.23	−0.66	−0.91	−1.46
	MmugDNA.12064.1.S1_at	CDKN2B	Cyclin-dependent kinase inhibitor 2B (p15, inhibits CDK4)	−1.13	−0.30	−0.04	−1.12
	MmugDNA.31081.1.S1_at	DAZAP2	DAZ associated protein 2	−1.27	−0.55	−1.06	−1.85
	MmugDNA.15195.1.S1_at	DBC1	Deleted in bladder cancer 1	0.06	−0.35	−1.26	−0.91
	MmugDNA.36289.1.S1_s_at	DLEU2 /// BCMSUNL	Deleted in lymphocytic leukemia, 2 /// BCMS upstream neighbor-like	0.32	0.45	0.74	**1.31**
	MmugDNA.16818.1.S1_at	DAB2	Disabled homolog 2, mitogen-responsive phosphoprotein (*Drosophila*)	−0.11	−0.14	−0.23	−1.01
	MmugDNA.32685.1.S1_at	DDR2	Discoidin domain receptor family, member 2	0.66	0.17	0.36	**1.52**
	MmugDNA.28062.1.S1_s_at	DLG1	Discs, large homolog 1 (*Drosophila*)	−0.14	−0.48	−0.39	−1.08
	MmugDNA.32495.1.S1_at	DDIT3	DNA-damage-inducible transcript 3	0.11	**1.30**	0.87	**1.32**
	MmugDNA.24043.1.S1_at	DUSP1	Dual specificity phosphatase 1	−1.04	−0.10	0.30	−0.04
	MmugDNA.23886.1.S1_at	DNCH1	Dynein, cytoplasmic, heavy polypeptide 1	0.66	0.73	0.35	**1.12**
	MmugDNA.13015.1.S1_at	EML4	Echinoderm microtubule associated protein like 4	**1.25**	0.32	0.32	**1.20**
	MmugDNA.38400.1.S1_at	ENTH	Enthoprotin	−1.06	−0.36	−0.37	−1.10
	MmugDNA.31099.1.S1_s_at	EPLIN	Epithelial protein lost in neoplasm beta	−0.78	−0.75	−1.34	−1.40
	MmugDNA.35735.1.S1_at	EPB41L4A	Erythrocyte membrane protein band 4.1 like 4A	−0.68	−0.41	−0.75	−1.43
	MmugDNA.29681.1.S1_at	FBXO45	F-box protein 45	0.91	0.26	0.40	**1.07**
	MmugDNA.25606.1.S1_s_at	FUS	Fusion (involved in t(12;16) in malignant liposarcoma)	−2.62	−0.90	−1.42	−1.31
	MmugDNA.7304.1.S1_s_at	GSPT1	G1 to S phase transition 1	−0.37	−0.31	−0.87	−1.50e
	MmugDNA.33793.1.S1_at	GTSE1	G-2 and S-phase expressed 1	**1.01**	−0.45	−0.19	0.08
	MmugDNA.33680.1.S1_at	GSN	Gelsolin (amyloidosis, Finnish type)	−1.14	0.00	−0.16	−0.89
	MmugDNA.38529.1.S1_at	ENPEP	Glutamyl aminopeptidase (aminopeptidase A)	−0.60	−0.43	−0.25	−1.08
	MmugDNA.25216.1.S1_at	GPC4	Glypican 4	−0.43	−0.59	−1.08	−1.42
	MmugDNA.41267.1.S1_at	GAS1	Growth arrest-specific 1	−0.16	0.13	−0.27	−1.40
	MmugDNA.23210.1.S1_x_at	IGF2	Insulin-like growth factor 2 (somatomedin A)	0.32	0.14	−0.89	−1.02
	MmugDNA.2176.1.S1_at	ISG20	Interferon stimulated exonuclease gene 20 kDa	0.09	0.19	0.43	**1.07**
	MmugDNA.18344.1.S1_at	JAG1	Jagged 1 (Alagille syndrome)	−0.10	−0.82	−1.04	−1.07
	MmugDNA.30627.1.S1_at	JUB	Jub, ajuba homolog (*Xenopus laevis*)	−0.68	−0.06	−0.27	−1.09
	MmugDNA.21869.1.S1_at	KIF22	Kinesin family member 22	−1.13	−0.37	−0.31	−1.16
	MmugDNA.17868.1.S1_at	MAD2L1	MAD2 mitotic arrest deficient-like 1 (yeast)	−1.17	−0.40	−0.22	−0.89
	MmugDNA.11043.1.S1_s_at	MAP7	Microtubule-associated protein 7	−0.34	−0.59	−0.58	−1.19
	MmugDNA.38080.1.S1_at	MPHOSPH9	M-phase phosphoprotein 9	−0.87	−0.77	−0.61	−1.50
	MmugDNA.40010.1.S1_at	NF2	Neurofibromin 2 (bilateral acoustic neuroma)	−0.40	0.02	−0.08	−1.13
	MmugDNA.11581.1.S1_at	NEK9	NIMA (never in mitosis gene a)-related kinase 9	−1.36	−0.42	−0.71	−1.71
	MmugDNA.25696.1.S1_at	NEK2	NIMA (never in mitosis gene a)-related kinase 2	−1.53	−0.80	−0.44	−1.37
	MmugDNA.15458.1.S1_at	NOTCH2	Notch homolog 2 (*Drosophila*)	−0.96	−0.30	−0.40	−1.14
	MmugDNA.31795.1.S1_at	NUCKS1	Nuclear casein kinase and cyclin-dependent kinase substrate 1	−1.19	−0.82	−1.07	−0.43
	MmugDNA.18184.1.S1_at	PAK3	P21 (CDKN1A)-activated kinase 3	**1.40**	0.09	0.17	**1.52**
	MmugDNA.6179.1.S1_at	PARD6B	Par-6 partitioning defective 6 homolog beta (C. elegans)	−1.09	−0.32	−0.55	−0.95
	MmugDNA.28892.1.S1_at	PPIG	Peptidylprolyl isomerase G (cyclophilin G)	**1.14**	0.00	−0.02	0.51

Table 1 (continued)

Categories and subcategories	Probe set ID	Gene symbol	Description	Log 2 ratio (sample/control)[a] (h p.i.)			
				12	24	48	72
Apoptosis							
Cell cycle and proliferation							
	MmugDNA.30055.1.S1_at	PAFAH1B1	Platelet-activating factor acetylhydrolase, isoform Ib, alpha subunit 45 kDa	−1.03	−0.40	−0.51	−1.19
	MmugDNA.27441.1.S1_at	PPP2R1B	Protein phosphatase 2 (formerly 2A), regulatory subunit A (PR 65), beta isoform	−1.02	−0.37	−0.47	−0.79
	MmugDNA.3729.1.S1_at	RIF1	RAP1 interacting factor homolog (yeast)	−1.76	−0.49	−0.70	−1.64
	MmugDNA.23090.1.S1_at	RERG	RAS-like, estrogen-regulated, growth inhibitor	−0.67	−0.43	−1.40	−2.26
	MmugDNA.24655.1.S1_s_at	RBBP6	Retinoblastoma binding protein 6	0.77	0.33	0.27	**1.01**
	MmugDNA.1893.1.S1_at	RNGTT	RNA guanylyltransferase and 5′-phosphatase	−1.06	−0.50	−0.51	−1.27
	MmugDNA.43216.1.S1_at	S100A6	S100 calcium binding protein A6 (calcyclin)	−0.20	−0.25	−0.30	−1.15
	MmugDNA.18017.1.S1_at	SEP2	Septin 2	−2.05	−0.63	−0.90	−2.10
	MmugDNA.7350.1.S1_s_at	SSR1	Signal sequence receptor, alpha (translocon-associated protein alpha)	−1.12	−0.04	0.23	−0.20
	MmugDNA.29506.1.S1_at	SMC5L1	SMC5 structural maintenance of chromosomes 5-like 1 (yeast)	0.81	0.27	0.06	**1.17**
	MmugDNA.10117.1.S1_s_at	SKP2	S-phase kinase-associated protein 2 (p45)	−1.68	−0.61	−0.65	−1.02
	MmugDNA.23385.1.S1_at	TSPAN2	Tetraspanin 2	−0.57	−0.51	−0.70	−1.07
	MmugDNA.39770.1.S1_at	TSPAN31	Tetraspanin 31	−0.80	−0.40	−0.24	−1.19
	MmugDNA.20960.1.S1_at	TGFA	Transforming growth factor, alpha	−1.50	−0.17	−0.44	−1.39
	MmugDNA.35789.1.S1_at	TUSC2	Tumor suppressor candidate 2	−0.71	−0.11	−0.22	−1.03
	MmugDNA.40025.1.S1_at	UHMK1	U2AF homology motif (UHM) kinase 1	−1.38	−0.36	−0.60	−1.80

[a] The bolded numbers represent genes with more than two-fold up-regulation, while the italicized numbers represent genes with more than two-fold down-regulation.

Differential gene expression confirmed by real-time PCR

To verify the result of the microarray analysis, relative expression levels of selected genes were assayed with real-time quantitative PCR. The relative quantification by real-time PCR suggested the creditability of the array analysis (Table 2). It is noted that the scale of expression level detected by these two systems may vary, possibly due to the variation of probing regions, sensitivity of assays, as well as the saturation of fluorescence signals in array analysis.

Transcriptional inactivation of extrinsic apoptotic pathway

Apoptosis is initiated through two interrelated pathways, one involving the engagement of TNF family of death receptors, namely the extrinsic pathway, and the other involving Bax-mediated release of cytochrome *c* (CYCS) from mitochondria, namely the intrinsic pathway. In the extrinsic pathway, engagement of death receptors have been shown to trigger the activation of MAPK/JNK, caspase 8 and caspase 3, which leads to apoptosis (Baetu and Hiscott, 2002). Based on our microarray data, expression of a number of genes involved in the extrinsic pathways of apoptosis was down-regulated. TRAIL, which is a ligand of death receptor 4/5 and a potent apoptotic inducer, and FAF1, which binds to FAS antigen and initiates apoptosis, were both found to be down-regulated upon S2 over-expression. These observations suggest a possible suppression of TRAIL-induced and FasL-induced apoptotic pathways. A downstream target of these two pathways, caspase 8, was also down-regulated at 48 and 72 h p.t. Although the down-regulation of HIPK3, a gene that activates the Fas apoptotic pathway (Curtin and Cotter, 2004), was observed, the possibility that the effect of

HIPK3 as a feedback mechanism cannot be excluded. Inhibition of apoptosis is a common strategy employed by viruses to evade host defense mechanism that limits viral replication by triggering the apoptosis of the infected cells (Hiscott et al., 2001). From this, the blockage of extrinsic apoptotic pathway by S2 may represent a viral defense mechanism to avoid premature cell death before the completion of viral replication.

Transcriptional activation of intrinsic apoptotic pathway

In our study, several lines of evidence suggest the triggering of intrinsic apoptotic pathway in response to S2 expression. From the microarray data, the expression of Mdm2, a protein

Table 2

Comparison of the gene expression levels in S2-expressing Vero E6 cells analyzed with microarray and real-time PCR

Gene name	Microarray[a]				Real time[b]			
	12	24	48	72	12	24	48	72
ATF1	−1.47	−0.47	−0.50	−1.24	−1.13	−0.15	−0.10	−1.63
Bcl−xL	−1.56	−0.23	−0.77	−1.92	−0.87	−0.58	−0.22	−1.73
CDK6	−1.23	−0.66	−0.91	−1.46	−0.50	−0.08	−1.00	−1.98
CYCS	**1.50**	0.58	0.40	**1.63**	**1.03**	0.62	0.45	**1.02**
GRP78	0.15	0.39	**1.88**	**2.15**	−0.26	0.67	**1.44**	**1.84**
GRP94	0.16	0.42	**1.41**	**1.15**	0.41	0.23	0.96	**1.21**
IGF2	0.32	0.14	−0.89	−1.02	0.65	0.58	−1.83	−2.28
IkBkB	−1.10	−0.56	−0.58	−0.76	−1.02	0.32	−0.13	−0.55
JunD	−0.27	0.01	0.22	−1.00	−0.85	−0.32	0.17	−1.12
MAPK1	−1.41	−0.32	−0.27	−1.42	−1.22	−0.83	0.52	−2.80

For both assays, bolded numbers represent genes with more than two-fold up-regulation, while italicizec numbers represent genes with more than two-fold down-regulation.

[a] For each gene, only the probe set with the largest variation is shown.

[b] The average expression level of triplicate experiments is shown.

that mediates the degradation of pro-apoptotic tumor suppressor protein p53 (Momand et al., 1992), was showed to be down-regulated. The down-regulation of Mdm2 thus suggests the possible increase of the activity of a pro-apoptotic Bcl-2 family member, Bax, via p53 (Miyashita and Reed, 1995). Bax accelerates the opening of the mitochondrial porin channel and mediates the release of CYCS (Narita et al., 1998). Indeed, as indicated in our data, the expression of S2 did up-regulate the transcription of CYCS, the leakage of CYCS is thus expected to be increased, which enables the formation of apoptosome and the subsequent activation of the downstream effector caspase cascade, and ultimately leads to apoptosis (Cain et al., 2002). Collectively, these data suggest that the intrinsic apoptotic pathway may possibly be responsible for the S2-induced apoptosis in Vero E6 cells.

In SARS-CoV-infected cells, down-regulation of Bcl-2 and up-regulation of Bax has been reported (Ren et al., 2005). These, together with the capacity of Bcl-2 to overcome the apoptotic effects of SARS-CoV (Bordi et al., 2006), imply the involvement of the intrinsic apoptotic pathway. In our array data, despite the fact that a pro-apoptotic member of the Bcl-2 family, Bim (Marani et al., 2002), was down-regulated, a number of anti-apoptotic Bcl-2 family members, including Mcl-1, Bcl-xL and Bcl-2 (Gross et al., 1999; Reed, 1996), were also found to be down-regulated. These anti-apoptotic members are known to inhibit the release of CYCS from mitochondria to cytosol by blocking the mitochondrial porin channel (Shimizu et al., 1999). To further elucidate the possible inhibitory role of the anti-apoptotic Bcl-2 protein members in S2-induced apoptosis, we over-expressed Bcl-xL in Vero E6 cells through rAd transduction. As shown in Fig. 3, over-expression of Bcl-xL significantly reduced the extent of apoptosis in Vero E6 cells induced by both S2 and S. In contrast, co-transduction of rAd-Ctrl with rAd-S2 or rAd-S has no significant effect on the level of apoptosis mediated by S nor S2 (data not shown). Besides the important role of Bcl-xL in mitochondrial apoptosis, it is noted that over-expression of Bcl-xL may inhibit other mitochondria-independent apoptotic pathways like phosphorylation of JNK (Srivastava et al., 1999).

Induction of endoplasmic reticulum stress responses

The expression of full length spike protein has been demonstrated to induce specific ER stress and unfolded protein response (UPR) while other viral proteins like M, N and E do not (Chan et al., 2006). Previous reports showed that ER stress may trigger 3 branches of UPR including activating transcription factor 6 (ATF6), inositol-requiring enzyme 1 (IRE1) and PKR-like ER kinase (PERK)-related signaling pathways (Schroder and Kaufman, 2005). Chan et al. (2006) demonstrated the ER stress induced by spike protein does not trigger ATF6 and IRE1-related signaling pathways while GRP78 and GRP94, indicators for activation of PERK-related signaling pathways (Schroder and Kaufman, 2005), are up-regulated. Interestingly, our array data on the expression of these genes, as well as the real-time PCR analysis of GRP78 and GRP94 expression (Table 2), are consistent with these findings, suggesting a possible role of the S2 subunit in the specific ER stress induced by S. Although GRP78/
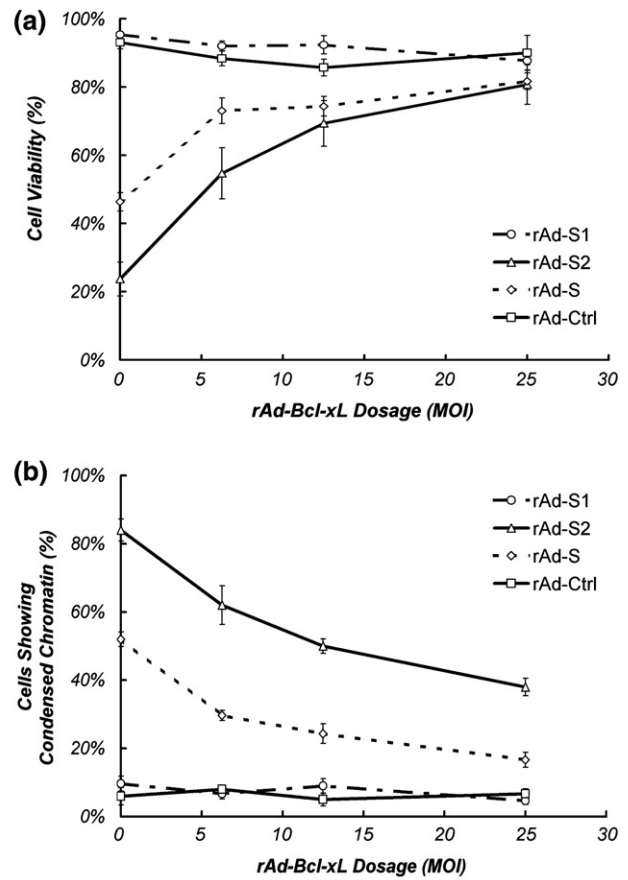

Fig. 3. Bcl-xL blocks S2-induced apoptosis in Vero E6 cells. Different dosage of rAd-Bcl-xL was co-infected with 50 MOI of rAd-S, -S1, -S2 or rAd-Ctrl and the effect on cell death and apoptosis induced by the rAds were assayed through (a) Trypan blue exclusion assay and (b) Hoechst 33342 staining at day 5 and day 3 p.t. respectively. Both figures indicated the average of three independent experiments with SEM.

94-induced UPR takes part in alleviating ER stress and promoting anti-apoptotic signaling (Ma and Hendershot, 2004), a prolonged ER stress may induce mitochondrial apoptosis by releasing calcium ion and down-regulating Bcl-2 (Breckenridge et al., 2003). Coincidentally, Bcl-2 was found to be down-regulated in this study (Table 1). ER stress may also activate caspase 4, which is a homologue to murine caspase 12 (Hitomi et al., 2004), to induce mitochondria-independent apoptotic response. However, due to the fact that murine caspase 12 is triggered through IRE1 activation (Yoneda et al., 2001) and that the over-expression of spike protein does not activate IRE1 (Chan et al., 2006), it is anticipated that caspase 4 may not be activated by SARS-CoV spike protein. Taken together, since a similar transcriptional response was observed by the expression of S of both SARS-CoV and MHV but not other viral proteins (Chan et al., 2006; Versteeg et al., 2007), we proposed that the potential ER stress observed in our assay is specific to S2 expression.

Inactivation of the NFκB pathway

The transcription factor NFκB is a key regulator in cell proliferation, protecting cells from apoptosis under most circumstances and accelerating apoptosis in the others (Piva et al.,

2006). Our data suggest a possible inhibition of NFκB activities, as supported by the regulation of several targets and regulators of NFκB. In particular, IκBκB, which is responsible for the activation of NFκB (Scheidereit, 2006), was down-regulated at the early time-point upon S2 expression. In addition, at both early (12 h p.t.) and late (72 h p.t.) time points, a negative regulator of NFκB, the TNFAIP3 (Wertz et al., 2004), was up-regulated, while positive regulators, including ECT2, FKBP1A, TRAIL, TMEM9B and TRIM38 (Matsuda et al., 2003), were down-regulated. NFκB-dependent decrease of the expression level of anti-apoptotic factors like Bcl-2 (Catz and Johnson, 2001), Bcl-xL (Chen et al., 2000), Mcl-1 (Henson et al., 2003), A1/Bfl-1 and TRAF-1 (Akari et al., 2001) has been demonstrated.

Down-regulation of the MAPK pathway

The MAPK-dependent signaling cascade is known to be important for regulating apoptosis, cell differentiation and proliferation. Potential suppression of the MAPK pathways is suggested to be mediated by the down-regulation of its key members, p38 MAPK (MAPK1) and p38 MAPKα (MAPK14), and the key targets, including ATF1 (Tan et al., 1996), CREB1 (Tan et al., 1996), JunD (Stocco et al., 2002) and Sp1 (Moon et al., 2006). While their transcriptional profiles have not been investigated in SARS-CoV-infected cells, based on our microarray results, we anticipate a conceivable role of S2 in down-regulating these genes at the transcription level. Suppression of MAPK cascade by S2 may imply various downstream responses as suggested by its overall regulation observed in other cell types. Consequential down-regulations of ATF1, CREB1, JunD and Sp1 observed in S2-expressing Vero E6 cells suggested the trend towards cell death. It is noted that the p38 MAPK, CREB, MSK-1, ERK1/2 and ATF1 (Mizutani et al., 2004b), and PI3k/Akt-dependent pathways (Mizutani et al., 2004a) were activated in SARS-CoV-infected Vero E6 cells, although their role in S2-mediated apoptosis has not yet been defined. Indeed, the activation of these proteins may possibly due to the presence of other viral proteins or the double-stranded RNA intermediates of SARS-CoV through different machineries (Mizutani et al., 2004b).

Transcriptional regulation of genes involved in cell cycle control

Cell cycle progression is mainly governed by proteins including cyclins, cyclin-dependent kinase (CDK) and CDK inhibitors, which cooperatively control the phosphorylation of retinoblastoma (Rb) (Sherr, 1996). The cyclin E2 (CCN E2)/ CDK6 complex is important for the progression of cell cycle in the G1/S phase. While IGF2 acts upstream of the complex (Zhang et al., 1999), the activity of CTNN B1 is regulated by the complex through binding (Park et al., 2004). MDM2 is a negative regulator of p53 and it has been demonstrated to inhibit the G1 arrest (Chen et al., 1996). The reduced MDM2 expression was expected to activate the inhibitor of CDKN 1A (p21, Cip1) via p53 (Waldman et al., 1995). In this study, transcriptional regulations of a number of cyclins, CDKs and their

inhibitors were detected. Cyclin D1 (CCN D1) was found to be up-regulated, while the expressions of IGF2, CCN E2, CDK6 and CTNN B1 were all suppressed upon S2 over-expression. CDKN 2B, a CDK inhibitor involved in negative regulation of cell proliferation, was also found to be down-regulated (Table 1). Thus, our data suggest the possibility of cell cycle arrest in G1/S phase by S2 through modulating G1 controlling cyclins. While the regulation of cell cycle mediators leading to cell proliferation inhibition is a common phenomenon in virus infection cycle, we observed, as described above, an inhibition of cell proliferation in cells transduced with rAd-S2 (Fig. 4). Further study to confirm the S2-induced arrest at G1/S phase will be indicative to understand the role of S2 in the pathogenesis of SARS-CoV.

It has been shown that SARS-CoV can induce cell proliferation arrest (Mizutani et al., 2006). Recent studies suggested the induction of G0/G1 phase arrest by SARS-CoV ORF 3b and 7a (Yuan et al., 2005; Yuan et al., 2006) and S phase arrest by N protein (Surjit et al., 2006). While the phase in which cell cycle is arrested in SARS-CoV-infected cells remained to be determined, the inhibition of G1 phase progression in mouse hepatitis virus (MHV) p28 protein-transduced (Chen et al., 2004) and in IBV-infected (Dove et al., 2006) cells with increase viral protein productions suggested the possible role of potential G1 arrest in rAd-S2-transduced cells. This in turn
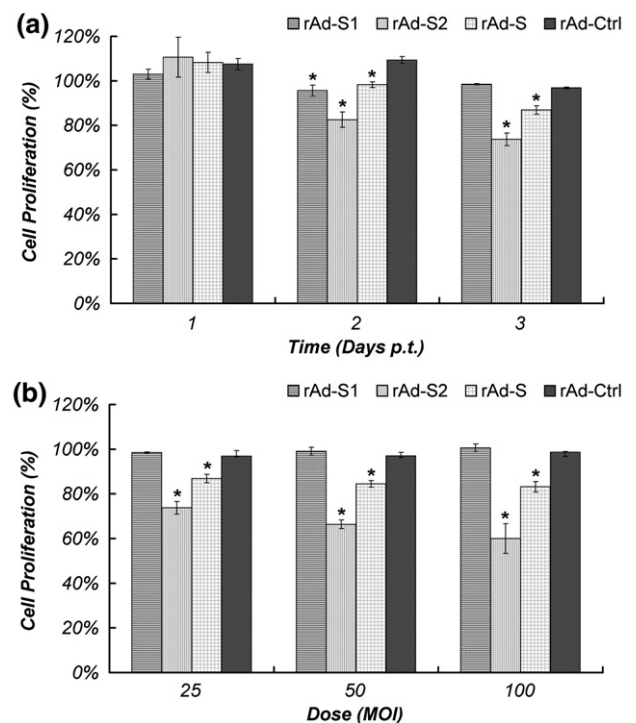

Fig. 4. S2-mediated inhibition of cell proliferation in Vero E6 cells. Vero E6 cells were transduced with the indicated rAds and their proliferations were estimated with MTT cell proliferation assay and are expressed as percentage of proliferation of mock-infected cells. Time- and dose-dependent anti-proliferation effect of S2 was shown in panels a and b, respectively. The time-dependent effect was performed with rAd of 25 MOI and cells in the dose-dependent experiment were collected at 3 days p.t. Results shown are the average of three independent experiments with SEM. *$p < 0.01$ when compared with cells transduced by rAd-Ctrl under the same condition.

plays a role in the lytic replication cycle, driving the infected cells to apoptosis showing cytopathic effect.

Overall conclusive remarks

In this study, we investigated the possible modulation of the host cellular factors by S2 of SARS-CoV, which may be important in mediating cell death and cell proliferation arrest. We observed a suppression of extrinsic apoptotic pathway and an activation of intrinsic pathway. Together with the down-regulation of genes involved in the MAPK and NFκB signaling pathway, these changes are believed to be responsible for the S2-induced apoptotic cell death. Modulation of expression of G1 cyclins also suggests the capacity of inducing G1 cell cycle arrest by S2. These data collectively elucidate the possible role of S2 in disease pathogenesis and viral replication. In summary, our investigation unraveled the candidate physiological pathways involved in S2-induced apoptosis at a molecular level, providing a foundation for researchers to design experiments based on testable hypothesis targeting individual genes. This information is expected to shed light on the molecular mechanisms of the pathogenesis of SARS, which is important for the development of antiviral therapy.

Materials and methods

Cell cultures

HEK293-derived AD-293 cells (Stratagene) used to propagate recombinant adenoviruses (rAds), and the African green monkey kidney cell line Vero E6 cells (CRL-1586, American Type Culture Collection) used for adenoviral transduction and microarray analysis were cultured and maintained as described (Chow et al., 2005).

Preparation of recombinant adenoviruses and transduction of Vero E6 cells

Recombinant adenoviruses expressing S (rAd-S), S1 (rAd-S1) and S2 (rAd-S2), as well as a control rAd with no transgene (rAd-Ctrl), were constructed, propagated, purified and titrated as previously described (Chow et al., 2005). For all adenoviral transductions in this study, monolayer of Vero E6 cells was infected with minimal volume of purified rAds at a multiplicity of infections (MOI) of 100 unless otherwise specified. At 2 h p.t., minimum essential medium with eagle's salts (EMEM; Gibco-BRL) was added to the transduced cells at a final concentration of 1% heat-inactivated fetal bovine serum (FBS; Gibco-BRL) and 1% antibiotics–antimycotic (Gibco-BRL).

Assessment of apoptosis induced by S2 expression

Cell viability, nuclear morphology and the extent of DNA fragmentation of rAd-S2 and rAd-Ctrl-transduced Vero E6 cells were investigated at the indicated time intervals using Trypan blue exclusion assay, Hoechst 33342 staining (Sigma) and genomic DNA laddering assay, respectively. All three assays were performed in triplicate as previously described (Chow et al., 2005).

RNA sample preparation and microarray analysis

To identify the differentially expressed transcripts induced by S2 expression, the global gene expression profiles of rAd-Ctrl and rAd-S2-transduced Vero E6 cells at 12, 24, 48 and 72 h p.t. were compared using GeneChip® Rhesus Macaque Genome Array (Affymetrix). The microarray was spotted with 52,865 probe sets referring to more than 47,000 *Macaca mulatta* transcripts. For both rAd-Ctrl and rAd-S2-transduced cells, total RNA were extracted from approximately 5×10^6 cells at each of the 4 indicated time points using RNeasy Mini Kit (Qiagen) according to manufacturer's instructions. The integrity of the extracted RNA was confirmed by electrophoresis in a 1% denaturing agarose gel and the aliquots were stored at -80 °C until further use. Fifteen micrograms of the extracted RNA from each sample at each of the time points was used in microarray analysis. Standard sample preparation using the one cycle target labeling system, slide hybridization and scanning was performed in the Institute of Systems Biology (ISB; Seattle, USA) according to manufacturer's instructions. The intensity value was then processed with RMAExpress for background adjustment, quartile normalization and summarization with the Web-based SEBAMS system. The physiological functions of the transcripts were annotated according to the original annotation of the array, iHOP database (Robert Hoffmann) and NetAffy database (Affymetrix).

Real-time quantitative PCR

Real-time quantitative PCR analysis was performed to validate the transcript expression pattern detected in the microarray for selected transcripts ($n=6$) using specific primers (Table 3). First strand cDNA was synthesized from 2 μg of the extracted RNA at each of the time point using MMLV-reverse transcriptase

Table 3
List of primers for quantitative real-time PCR analysis

	Primer name	Primer sequence (5′-3′)	Product size
1	β-Actin_F	ATCGTGCGTGACATTAAGGAG	179
	β-Actin_R	AGGAAGGAAGGCTGGAAGAG	
2	ATF1_F	CAGGCACAGATGGAGTACAG	131
	ATF1_R	CTGATTGCTGGGCACAAGTA	
3	Bcl-xL_F	TTGAACAGGTAGTGAATGAACTC	139
	Bcl-xL_R	AAGCTGCGATCCGACTCACC	
4	CDK6_F	CCGAAGTCTTGCTCCAGTC	124
	CDK6_R	CCTAGTTGATCGACATCTGAA	
5	CYCS_F	TCCACATGGCTGTCAAGAA	113
	CYCS_R	CACGACGCCCAGTTATCTA	
6	GRP78_F	GGCAACTGGCTGAAAGGT	92
	GRP78_R	GGCAGTGCAGCAGAGGTC	
7	GRP94_F	CGCTTCGGTCAGGATATC	151
	GRP94_R	CTGTCGTGTCTTCTGTTGTCT	
8	IGF2_F	GTCCAGCAATCGGAAGTGA	125
	IGF2_R	GGAAGTGGAACCGAGAGATT	
9	IkBkB_F	GCAGCAAGGAGAACAGAGG	152
	IkBkB_R	CGACGGTCACTGTGTACTTCT	
10	JunD_F	CCTCAAGAGTCAGAACACGGA	98
	JunD_R	CGCTGTTGACGTGGCTGA	
11	MAPK1_F	CATCGCCGAAGCACCATT	108
	MAPK1_R	CTGTATCCTGGCTGGAATCT	

(Promega) according to manufacturer's instructions. Real-time PCR analysis was then performed with the EvaGreen real-time PCR system (Biotium Inc.) and the iCycler real-time PCR machine (Bio-Rad) according to the manufacturers' instructions. The amplification cycle included initial denaturation at 94 °C 10 min and 45 cycles of (94 °C 10 s, 55 °C 10 s, 72 °C 10 s, 80 °C 7 s), followed by 76 cycles of (+0.5 °C per s) from 56 °C for melting curve analysis. Amplification of the specific genes was repeated in triplicate. The relative expression (RE) of each gene in rAd-transduced cells were calculated relative to that of β-actin ($RE_{\beta\text{-actin}}$) using the ΔCt method, i.e. $RE_{\beta\text{-actin}} = 2^{\Delta Ct}$, while $\Delta Ct = (Ct_{\beta\text{-actin}} - Ct_{\text{target gene}})$. The normalized results were represented as the number of fold changes when compared to the rAd-Ctrl in each time point, which was calculated as log 2 [$RE_{\beta\text{-actin}}$ (rAd-S2 transduced)] log2 [$RE_{\beta\text{-actin}}$ (rAd-Ctrl transduced)]$^{-1}$.

MTT cell proliferation assay

Cell proliferation in rAd-transduced Vero E6 cells was evaluated in a time- and dose-dependent manner using MTT Cell Proliferation Kit (Roche) according to manufacturer's instructions. Briefly, 1×10^4 Vero E6 cells were seeded in each well of a 96-well tissue culture plate (Falcon) 1 day before rAd transduction at the indicated MOIs. To assess the extent of cell proliferation, MTT labeling reagent was added in the indicated time points at a final concentration of 0.5 mg ml^{-1} and the plate was incubated at 37 °C in dark for 4 h before the addition of solubilization solution. The plate was then allowed to stand overnight before the measurement of absorbance at 595 nm.

Bcl-xL co-transduction assay

Recombinant adenovirus carrying Bcl-xL (rAd-Bcl-xL) was cloned, propagated and purified in the same way of other rAds as described, whereas the Bcl-xL transgene was cloned from the cDNA of Vero E6 cells. The expression of Bcl-xL in rAd-Bcl-xL-transduced Vero E6 cells was confirmed by Western blot targeting the transgene's V5 tag (data not shown). Ten thousand cells were seeded 1 day before transduction. Serial diluted rAd-Bcl-xL was then added to the cells 30 min before the transduction of other candidate rAds at 50 MOI. After an incubation for another 1.5 h, EMEM was added to each well to achieve a final concentration of 1% FBS.

Acknowledgment

References

Akari, H., Bour, S., Kao, S., Adachi, A., Strebel, K., 2001. The human immunodeficiency virus type 1 accessory protein Vpu induces apoptosis by suppressing the nuclear factor kappaB-dependent expression of antiapoptotic factors. J. Exp. Med. 194 (9), 1299–1311.

Baetu, T.M., Hiscott, J., 2002. On the TRAIL to apoptosis. Cytokine Growth Factor Rev. 13 (3), 199–207.

Bordi, L., Castilletti, C., Falasca, L., Ciccosanti, F., Calcaterra, S., Rozera, G., Di Caro, A., Zaniratti, S., Rinaldi, A., Ippolito, G., Piacentini, M., Capobianchi, M.R., 2006. Bcl-2 inhibits the caspase-dependent apoptosis induced by SARS-CoV without affecting virus replication kinetics. Arch. Virol. 151 (2), 369–377.

Breckenridge, D.G., Germain, M., Mathai, J.P., Nguyen, M., Shore, G.C., 2003. Regulation of apoptosis by endoplasmic reticulum pathways. Oncogene 22 (53), 8608–8618.

Cain, K., Bratton, S.B., Cohen, G.M., 2002. The Apaf-1 apoptosome: a large caspase-activating complex. Biochimie. 84 (2–3), 203–214.

Catz, S.D., Johnson, J.L., 2001. Transcriptional regulation of bcl-2 by nuclear factor kappa B and its significance in prostate cancer. Oncogene 20 (50), 7342–7351.

Chan, C.P., Siu, K.L., Chin, K.T., Yuen, K.Y., Zheng, B., Jin, D.Y., 2006. Modulation of the unfolded protein response by the severe acute respiratory syndrome coronavirus spike protein. J. Virol. 80 (18), 9279–9287.

Chen, J., Wu, X., Lin, J., Levine, A.J., 1996. mdm-2 inhibits the G1 arrest and apoptosis functions of the p53 tumor suppressor protein. Mol. Cell. Biol. 16 (5), 2445–2452.

Chen, C., Edelstein, L.C., Gelinas, C., 2000. The Rel/NF-kappaB family directly activates expression of the apoptosis inhibitor Bcl-x(L). Mol. Cell. Biol. 20 (8), 2687–2695.

Chen, C.J., Sugiyama, K., Kubo, H., Huang, C., Makino, S., 2004. Murine coronavirus nonstructural protein p28 arrests cell cycle in G0/G1 phase. J. Virol. 78 (19), 10410–10419.

Chow, K.Y., Yeung, Y.S., Hon, C.C., Zeng, F., Law, K.M., Leung, F.C., 2005. Adenovirus-mediated expression of the C-terminal domain of SARS-CoV spike protein is sufficient to induce apoptosis in Vero E6 cells. FEBS Lett. 579 (30), 6699–6704.

Curtin, J.F., Cotter, T.G., 2004. JNK regulates HIPK3 expression and promotes resistance to Fas-mediated apoptosis in DU 145 prostate carcinoma cells. J. Biol. Chem. 279 (17), 17090–17100.

Dimitrov, D.S., 2004. Virus entry: molecular mechanisms and biomedical applications. Nat. Rev., Microbiol. 2 (2), 109–122.

Dove, B., Brooks, G., Bicknell, K., Wurm, T., Hiscox, J.A., 2006. Cell cycle perturbations induced by infection with the coronavirus infectious bronchitis virus and their effect on virus replication. J. Virol. 80 (8), 4147–4156.

Drosten, C., Gunther, S., Preiser, W., van der Werf, S., Brodt, H.R., Becker, S., Rabenau, H., Panning, M., Kolesnikova, L., Fouchier, R.A., Berger, A., Burguiere, A., Cinatl, M., Eickmann, J., Escriou, M., Grywna, N., Kramme, K., Manuguerra, S., Muller, C., Rickerts, S., Sturmer, V., Vieth, M., Klenk, S., Osterhaus, H.D., Schmitz, A.D., Doerr, H., 2003. Identification of a novel coronavirus in patients with severe acute respiratory syndrome. N. Engl. J. Med. 348 (20), 1967–1976.

Duan, J., Yan, X., Guo, X., Cao, W., Han, W., Qi, C., Feng, J., Yang, D., Gao, G., Jin, G., 2005. A human SARS-CoV neutralizing antibody against epitope on S2 protein. Biochem. Biophys. Res. Commun. 333 (1), 186–193.

Gross, A., McDonnell, J.M., Korsmeyer, S.J., 1999. BCL-2 family members and the mitochondria in apoptosis. Genes Dev. 13 (15), 1899–1911.

Hattermann, K., Muller, M.A., Nitsche, A., Wendt, S., Donoso Mantke, O., Niedrig, M., 2005. Susceptibility of different eukaryotic cell lines to SARS-coronavirus. Arch. Virol. 150 (5), 1023–1031.

He, M.L., Zheng, B.J., Chen, Y., Wong, K.L., Huang, J.D., Lin, M.C., Peng, Y., Yuen, K.Y., Sung, J.J., Kung, H.F., 2006. Kinetics and synergistic effects of siRNAs targeting structural and replicase genes of SARS-associated coronavirus. FEBS Lett. 580 (10), 2414–2420.

Henson, E.S., Gibson, E.M., Villanueva, J., Bristow, N.A., Haney, N., Gibson, S.B., 2003. Increased expression of Mcl-1 is responsible for the blockage of TRAIL-induced apoptosis mediated by EGF/ErbB1 signaling pathway. J. Cell. Biochem. 89 (6), 1177–1192.

Hiscott, J., Kwon, H., Genin, P., 2001. Hostile takeovers: viral appropriation of the NF-kappaB pathway. J. Clin. Invest. 107 (2), 143–151.

Hitomi, J., Katayama, T., Eguchi, Y., Kudo, T., Taniguchi, M., Koyama, Y., Manabe, T., Yamagishi, S., Bando, Y., Imaizumi, K., Tsujimoto, Y., Tohyama, M., 2004. Involvement of caspase-4 in endoplasmic reticulum stress-induced apoptosis and Abeta-induced cell death. J. Cell Biol. 165 (3), 347–356.

Hofmann, H., Pohlmann, S., 2004. Cellular entry of the SARS coronavirus. Trends Microbiol. 12 (10), 466–472.

Jamshidi-Parsian, A., Dong, Y., Zheng, X., Zhou, H.S., Zacharias, W., McMasters, K.M., 2005. Gene expression profiling of E2F-1-induced apoptosis. Gene 344, 67–77.

Kaye, M., 2006. SARS-associated coronavirus replication in cell lines. Emerg. Infect. Dis. 12 (1), 128–133.

Keng, C.T., Zhang, A., Shen, S., Lip, K.M., Fielding, B.C., Tan, T.H., Chou, C.F., Loh, C.B., Wang, S., Fu, J., Yang, X., Lim, S.G., Hong, W., Tan, Y.J., 2005. Amino acids 1055 to 1192 in the S2 region of severe acute respiratory syndrome coronavirus S protein induce neutralizing antibodies: implications for the development of vaccines and antiviral agents. J. Virol. 79 (6), 3289–3296.

Ksiazek, T.G., Erdman, D., Goldsmith, C.S., Zaki, S.R., Peret, T., Emery, S., Tong, S., Urbani, C., Comer, J.A., Lim, W., Rollin, P.E., Dowell, S.F., Ling, A.E., Humphrey, C.D., Shieh, W.J., Guarner, J., Paddock, C.D., Rota, P., Fields, B., DeRisi, J., Yang, J., Cox, Y., Hughes, N., LeDuc, J.M., Bellini, J.W., Anderson, W.J., 2003. A novel coronavirus associated with severe acute respiratory syndrome. N. Engl. J. Med. 348 (20), 1953–1966.

Lai, C.W., Chan, Z.R., Yang, D.G., Lo, W.H., Lai, Y.K., Chang, M.D., Hu, Y.C., 2006. Accelerated induction of apoptosis in insect cells by baculovirus-expressed SARS-CoV membrane protein. FEBS Lett. 580 (16), 3829–3834.

Law, P.T., Wong, C.H., Au, T.C., Chuck, C.P., Kong, S.K., Chan, P.K., To, K.F., Lo, A.W., Chan, J.Y., Suen, Y.K., Chan, H.Y., Fung, K.P., Waye, M.M., Sung, J.J., Lo, Y.M., Tsui, S.K., 2005. The 3a protein of severe acute respiratory syndrome-associated coronavirus induces apoptosis in Vero E6 cells. J. Gen. Virol. 86 (Pt 7), 1921–1930.

Leong, W.F., Tan, H.C., Ooi, E.E., Koh, D.R., Chow, V.T., 2005. Microarray and real-time RT-PCR analyses of differential human gene expression patterns induced by severe acute respiratory syndrome (SARS) coronavirus infection of Vero cells. Microbes Infect. 7 (2), 248–259.

Ma, Y., Hendershot, L.M., 2004. The role of the unfolded protein response in tumour development: friend or foe? Nat. Rev., Cancer 4 (12), 966–977.

Marani, M., Tenev, T., Hancock, D., Downward, J., Lemoine, N.R., 2002. Identification of novel isoforms of the BH3 domain protein Bim which directly activate Bax to trigger apoptosis. Mol. Cell. Biol. 22 (11), 3577–3589.

Martina, B.E., Haagmans, B.L., Kuiken, T., Fouchier, R.A., Rimmelzwaan, G.F., Van Amerongen, G., Peiris, J.S., Lim, W., Osterhaus, A.D., 2003. Virology: SARS virus infection of cats and ferrets. Nature 425 (6961), 915.

Matsuda, A., Suzuki, Y., Honda, G., Muramatsu, S., Matsuzaki, O., Nagano, Y., Doi, T., Shimotohno, K., Harada, T., Nishida, E., Hayashi, H., Sugano, S., 2003. Large-scale identification and characterization of human genes that activate NF-kappaB and MAPK signaling pathways. Oncogene 22 (21), 3307–3318.

Miyashita, T., Reed, J.C., 1995. Tumor suppressor p53 is a direct transcriptional activator of the human bax gene. Cell 80 (2), 293–299.

Mizutani, T., Fukushi, S., Saijo, M., Kurane, I., Morikawa, S., 2004a. Importance of Akt signaling pathway for apoptosis in SARS-CoV-infected Vero E6 cells. Virology 327 (2), 169–174.

Mizutani, T., Fukushi, S., Saijo, M., Kurane, I., Morikawa, S., 2004b. Phosphorylation of p38 MAPK and its downstream targets in SARS coronavirus-infected cells. Biochem. Biophys. Res. Commun. 319 (4), 1228–1234.

Mizutani, T., Fukushi, S., Iizuka, D., Inanami, O., Kuwabara, M., Takashima, H., Yanagawa, H., Saijo, M., Kurane, I., Morikawa, S., 2006. Inhibition of cell proliferation by SARS-CoV infection in Vero E6 cells. FEMS Immunol. Med. Microbiol. 46 (2), 236–243.

Momand, J., Zambetti, G.P., Olson, D.C., George, D., Levine, A.J., 1992. The mdm-2 oncogene product forms a complex with the p53 protein and inhibits p53-mediated transactivation. Cell 69 (7), 1237–1245.

Moon, S.K., Choi, Y.H., Kim, C.H., Choi, W.S., 2006. p38MAPK mediates benzyl isothiocyanate-induced p21WAF1 expression in vascular smooth muscle cells via the regulation of Sp1. Biochem. Biophys. Res. Commun. 350 (3), 662–668.

Narita, M., Shimizu, S., Ito, T., Chittenden, T., Lutz, R.J., Matsuda, H., Tsujimoto, Y., 1998. Bax interacts with the permeability transition pore to induce permeability transition and cytochrome c release in isolated mitochondria. Proc. Natl. Acad. Sci. U. S. A. 95 (25), 14681–14686.

Park, C.S., Kim, S.I., Lee, M.S., Youn, C.Y., Kim, D.J., Jho, E.H., Song, W.K., 2004. Modulation of beta-catenin phosphorylation/degradation by cyclin-dependent kinase 2. J. Biol. Chem. 279 (19), 19592–19599.

Peiris, J.S., 2003. Severe acute respiratory syndrome (SARS). J. Clin. Virol. 28 (3), 245–247.

Piva, R., Belardo, G., Santoro, M.G., 2006. NF-kappaB: a stress-regulated switch for cell survival. Antioxid. Redox Signal 8 (3–4), 478–486.

Reed, J.C., 1996. Mechanisms of Bcl-2 family protein function and dysfunction in health and disease. Behring.-Inst.-Mitt. (97), 72–100.

Reghunathan, R., Jayapal, M., Hsu, L.Y., Chng, H.H., Tai, D., Leung, B.P., Melendez, A.J., 2005. Expression profile of immune response genes in patients with severe acute respiratory syndrome. BMC Immunol. 6, 2.

Ren, L., Yang, R., Guo, L., Qu, J., Wang, J., Hung, T., 2005. Apoptosis induced by the SARS-associated coronavirus in Vero cells is replication-dependent and involves caspase. DNA Cell Biol. 24 (8), 496–502.

Scheidereit, C., 2006. IkappaB kinase complexes: gateways to NF-kappaB activation and transcription. Oncogene 25 (51), 6685–6705.

Schroder, M., Kaufman, R.J., 2005. The mammalian unfolded protein response. Annu. Rev. Biochem. 74, 739–789.

Sherr, C.J., 1996. Cancer cell cycles. Science 274 (5293), 1672–1677.

Shimizu, S., Narita, M., Tsujimoto, Y., 1999. Bcl-2 family proteins regulate the release of apoptogenic cytochrome c by the mitochondrial channel VDAC. Nature 399 (6735), 483–487.

Srivastava, R.K., Sollott, S.J., Khan, L., Hansford, R., Lakatta, E.G., Longo, D.L., 1999. Bcl-2 and Bcl-X(L) block thapsigargin-induced nitric oxide generation, c-Jun NH(2)-terminal kinase activity, and apoptosis. Mol. Cell. Biol. 19 (8), 5659–5674.

Stocco, C.O., Lau, L.F., Gibori, G., 2002. A calcium/calmodulin-dependent activation of ERK1/2 mediates JunD phosphorylation and induction of nur77 and 20alpha-hsd genes by prostaglandin F2alpha in ovarian cells. J. Biol. Chem. 277 (5), 3293–3302.

Surjit, M., Liu, B., Jameel, S., Chow, V.T., Lal, S.K., 2004. The SARS coronavirus nucleocapsid protein induces actin reorganization and apoptosis in COS-1 cells in the absence of growth factors. Biochem. J. 383 (Pt 1), 13–18.

Surjit, M., Liu, B., Chow, V.T., Lal, S.K., 2006. The nucleocapsid protein of severe acute respiratory syndrome-coronavirus inhibits the activity of cyclin-cyclin-dependent kinase complex and blocks S phase progression in mammalian cells. J. Biol. Chem. 281 (16), 10669–10681.

Tan, Y., Rouse, J., Zhang, A., Cariati, S., Cohen, P., Comb, M.J., 1996. FGF and stress regulate CREB and ATF-1 via a pathway involving p38 MAP kinase and MAPKAP kinase-2. EMBO J. 15 (17), 4629–4642.

Tan, Y.J., Fielding, B.C., Goh, P.Y., Shen, S., Tan, T.H., Lim, S.G., Hong, W., 2004. Overexpression of 7a, a protein specifically encoded by the severe acute respiratory syndrome coronavirus, induces apoptosis via a caspase-dependent pathway. J. Virol. 78 (24), 14043–14047.

Tang, B.S., Chan, K.H., Cheng, V.C., Woo, P.C., Lau, S.K., Lam, C.C., Chan, T.L., Wu, A.K., Hung, I.F., Leung, S.Y., Yuen, K.Y., 2005. Comparative host gene transcription by microarray analysis early after infection of the Huh7 cell line by severe acute respiratory syndrome coronavirus and human coronavirus 229E. J. Virol. 79 (10), 6180–6193.

Versteeg, G.A., van de Nes, P.S., Bredenbeek, P.J., Spaan, W.J., 2007. The coronavirus spike protein induces ER stress and upregulation of intracellular chemokine mRNA concentrations. J. Virol. 81 (20), 10981–10990.

Waldman, T., Kinzler, K.W., Vogelstein, B., 1995. p21 is necessary for the p53-mediated G1 arrest in human cancer cells. Cancer Res. 55 (22), 5187–5190.

Wertz, I.E., O'Rourke, K.M., Zhou, H., Eby, M., Aravind, L., Seshagiri, S., Wu, P., Wiesmann, C., Baker, R., Boone, D.L., Ma, A., Koonin, E.V., Dixit, V.M., 2004. De-ubiquitination and ubiquitin ligase domains of A20 down-regulate NF-kappaB signalling. Nature 430 (7000), 694–699.

Wong, R.S., Wu, A., To, K.F., Lee, N., Lam, C.W., Wong, C.K., Chan, P.K., Ng, M.H., Yu, L.M., Hui, D.S., Tam, J.S., Cheng, G., Sung, J.J., 2003. Haematological manifestations in patients with severe acute respiratory syndrome: retrospective analysis. BMJ 326 (7403), 1358–1362.

Yan, H., Xiao, G., Zhang, J., Hu, Y., Yuan, F., Cole, D.K., Zheng, C., Gao, G.F., 2004. SARS coronavirus induces apoptosis in Vero E6 cells. J. Med. Virol. 73 (3), 323–331.

Yang, Y., Xiong, Z., Zhang, S., Yan, Y., Nguyen, J., Ng, B., Lu, H., Brendese, J., Yang, F., Wang, H., Yang, X.F., 2005. Bcl-xL inhibits T-cell apoptosis induced by expression of SARS coronavirus E protein in the absence of growth factors. Biochem. J. 392 (Pt 1), 135–143.

Yoneda, T., Imaizumi, K., Oono, K., Yui, D., Gomi, F., Katayama, T., Tohyama, M., 2001. Activation of caspase-12, an endoplastic reticulum (ER) resident caspase,

through tumor necrosis factor receptor-associated factor 2-dependent mechanism in response to the ER stress. J. Biol. Chem. 276 (17), 13935–13940.

Yu, S.Y., Hu, Y.W., Liu, X.Y., Xiong, W., Zhou, Z.T., Yuan, Z.H., 2005. Gene expression profiles in peripheral blood mononuclear cells of SARS patients. World J. Gastroenterol. 11 (32), 5037–5043.

Yuan, X., Shan, Y., Zhao, Z., Chen, J., Cong, Y., 2005. G0/G1 arrest and apoptosis induced by SARS-CoV 3b protein in transfected cells. Virol. J. 2, 66.

Yuan, X., Wu, J., Shan, Y., Yao, Z., Dong, B., Chen, B., Zhao, Z., Wang, S., Chen, J., Cong, Y., 2006. SARS coronavirus 7a protein blocks cell cycle progression at G0/G1 phase via the cyclin D3/pRb pathway. Virology 346 (1), 74–85.

Zeng, F., Hon, C.C., Yip, C.W., Law, K.M., Yeung, Y.S., Chan, K.H., Malik Peiris, J.S., Leung, F.C., 2006. Quantitative comparison of the efficiency of antibodies against S1 and S2 subunit of SARS coronavirus spike protein in virus neutralization and blocking of receptor binding: implications for the functional roles of S2 subunit. FEBS Lett. 580 (24), 5612–5620.

Zhang, H., Wang, G., Li, J., Nie, Y., Shi, X., Lian, G., Wang, W., Yin, X., Zhao, Y., Qu, X., Ding, M., Deng, H., 2004. Identification of an antigenic determinant on the S2 domain of the severe acute respiratory syndrome coronavirus spike glycoprotein capable of inducing neutralizing antibodies. J. Virol. 78 (13), 6938–6945.

Zhang, L., Kim, M., Choi, Y.H., Goemans, B., Yeung, C., Hu, Z., Zhan, S., Seth, P., Helman, L.J., 1999. Diminished G1 checkpoint after gamma-irradiation and altered cell cycle regulation by insulin-like growth factor II overexpression. J. Biol. Chem. 274 (19), 13118–13126.

Zhao, G., Shi, S.Q., Yang, Y., Peng, J.P., 2006. M and N proteins of SARS coronavirus induce apoptosis in HPF cells. Cell Biol. Toxicol. 22 (5), 313–322.

Zhong, N.S., Zheng, B.J., Li, Y.M., Xie, Z.H., Chan, K.H., Li, P.H., Tan, S.Y., Chang, Q., Xie, J.P., Liu, X.Q., Xu, J., Li, D.X., Yuen, K.Y., Guan, Y., 2003. Epidemiology and cause of severe acute respiratory syndrome (SARS) in Guangdong, People's Republic of China, in February, 2003. Lancet 362 (9393), 1353–1358.